Iris Recognition Based on Few-Shot Learning

Abstract

Iris recognition is a hot research field in the biometrics, and it plays an important role in automatic recognition. Given sufficient training data, some deep learning-based approaches have achieved good performance on iris recognition. However, when the training data are limited, the overfitting may occur. To address this issue, in this paper, we proposed a few-shot learning approach for iris recognition, based on model-agnostic meta-learning (MAML). To our best knowledge, we are the first to apply few-shot learning for iris recognition. Our experiments on the benchmark datasets have demonstrated that the proposed approach can achieve higher performance than the original MAML, and it is competitive to deep learning-based approaches.

Keywords: iris recognition, few-shot learning,

meta learning, L2 regularization

1.Introduction

Biometric systems are constantly evolving, and are expected to be used in automated systems to effectively identify or authenticate a person's identity without requiring the user to carry or remember anything, which is different from traditional methods such as passwords and IDs [1]. In this regard, iris recognition has been used in many key applications, such as restricted area access control, database access, national ID cards and financial services, and is considered to be one of the most reliable and accurate biometric features [2]. Several studies [3][4][5] have shown that iris features have many advantages over other biological features (such as face, fingerprint), which makes it widely recognized in biometric systems with high reliability and accuracy.

With the development of advanced computing hardware and the availability of big data, deep learning technologies have been applied to many areas, including iris recognition. In 2016, Gangwar and Joshi developed a deep learning architecture called DeepIrisNet [6] for iris recognition based on images obtained from different devices. Their experiments on the ND-IRIS-0405 and ND-CrossSensor-Iris-2013 datasets showed that the proposed network achieves better performance than the benchmarks. Zhao et al. proposed a deep learning method for iris recognition based on the capsule network architecture [7]. Wang et al. [8] proposed a cross-spectral iris recognition based on CNN and supervised discrete hashing. Compared with other iris recognition methods, the proposed method can not only achieve better performance than other considered CNN architectures, but also can significantly reduce the template size. Liu et al. [9] proposed two iris segmentation models based on hierarchical convolutional neural networks (HCNNs) and multi-scale full convolutional networks (MFCNs), for noisy iris images acquired at-a-distance and on-the-move. Both models automatically locate iris pixels without handcrafted features or rules, and they are end-to-end models which require no further pre- and post-processing and outperform other state-of-the-art methods.

When a sufficient amount of labeled data is available, the iris recognition approaches based on deep learning are able to achieve good performance. However, given a limited number of training samples, these methods may result in over-fitting.

To tackle the over-fitting problem, in recent years, the research on few-shot learning, i.e. learning for the problem of insufficient sample size, has attracted widespread attention [10]. In the context of iris recognition, though the overall sample size of datasets is considerable,

the specific iris images of each person are generally only about 20, which is relatively small compared to other types of datasets. Some deep learning-based methods [11] rotate the original iris images by various angles to expand the sample size. However, this approach does not increase the diversity between each sample and consequently has limited effects on preventing the over-fitting issue.

Inspired by the advantages of few-shot learning on addressing the issue caused by small samples, in this paper, we proposed a few-shot learning approach, based on the model-agnostic meta-learning method (MAML) [12]. We name the proposed approach as improved MAML, or iMAML. To adapt MAML for iris recognition, we have introduced L2 regularization on the basis of the original cross-entropy loss function, and increased the number of convolutional layers of the original network structure of MAML. To our best knowledge, we are the first to implore the few-shot learning for iris recognition. Our experiments on the benchmark datasets show that iMAML performs better than MAML and achieves competitive performance when compared with deep-learning based approaches.

The rest of this paper is organized as follows. The second section introduces the related work of iris recognition and few-shot learning. The third section introduces the preliminary knowledge of MAML. Section 4 introduces the improved algorithm proposed and provides the corresponding pseudo code. The experimental setup and results are reported in the fifth section, followed by the conclusions and future work.

2 Related work

A complete iris recognition system consists of several steps, including iris image acquisition, iris image quality evaluation, iris image preprocessing, iris feature extraction and recognition. In this section, we review traditional iris recognition approaches and deep-learning based ones.

2.1 Traditional approaches

The traditional iris recognition algorithm is mainly based on the theory of Daugman et al [13]. It uses Gabor filter to extract the feature of iris image texture and the iris feature extraction is completed by designing filter parameters, filter window size, filter direction and filter wavelength size. A series of feature coding work is carried out on the extracted iris features, and the feature code is edited for each type of iris image, and then the iris feature coding is compared with the coding in the iris registry. The matching algorithm of Haming distance and Euclidean distance is used for comparison. In 1997, Boles et al. [14] proposed an iris recognition algorithm based on wavelet zero-crossing detection. This method uses the idea of wavelet zero-crossing to extract features from the iris, which improves the efficiency of feature extraction. In 2001, [15] proposed a feature expression method based on two-dimensional wavelet transform for the problem of high iris feature dimension, which effectively reduced the dimension and improved the classification and recognition effect. In 2002, Tan et al. [16] proposed a personal recognition method based on iris recognition, which uses a row of circular symmetric filters to extract local iris features to form a fixed-length feature vector. At the same time, in order to improve the iris matching performance, constraints are imposed on the nearest feature line. In 2010, Mayank Vatsa et al. [17] used quality scores to select the two channels of color iris images and used redundant discrete wavelet transform to fuse them at the image level, before combing the fused image with the remaining channels at the scoring level.

2.2 Deep-learning based approaches

The iris recognition algorithm based on deep learning integrates iris feature extraction and iris matching, and performs iris feature extraction and iris matching through each layer of the network. On the premise of improving the recognition accuracy, it also improves the model's noise robustness and generalization ability. In 2016, Shervin Minaee et al. [18] used deep convolutional networks to extract features of iris images, and then used SVM as a classifier for iris recognition. In the same year, Abhishek Gangwar and Akanksha Joshi et al. proposed two CNN architectures, DeepIrisNet-A and DeepIrisNet-B for iris recognition. In 2017, Zhang et al. [19] proposed an iris recognition method based on a convolutional neural network, which consists of three convolutional

layers, three pooling layers, and two fully connected layers. The cross-entropy loss function is used to calculate the loss of the prediction result. In order to reduce the impact of overfitting, the Dropout method [20] is introduced into the network. In 2018, Wang et al. [21] used CNN to extract the depth feature vector of the normalized iris texture image as the underlying feature to classify the iris. Despite the good performance achieved by the above-mentioned approaches, they require big sample size to training their network models. Few-shot learning has been proposed to address the issue caused by small sample size, but it is not applied to iris recognition yet.

3. MAML

MAML [12] is a model-independent meta-learning algorithm that can be used for various learning problems and models based on gradient descent. Unlike the previous meta-learning method that requires learning an update function or learning rule, MAML neither increases the number of model parameters nor sets any restrictions on the structure of the model. MAML can easily interact with fully connected networks, convolutional networks, and recurrent networks, and so on.

The training of MAML algorithm takes task as the training unit, and the corresponding dataset is divided into training set, verification set and test set. The whole algorithm is divided into meta-training phase and meta-testing phase. In the meta-training phase, select the tasks from the given distributed $\mathcal{T}_i \sim p(\mathcal{T})$, where each task contains K categories, and each category contains N samples. Meta-learning tries to obtain a good generalized model by training all tasks, which can quickly adapt to new tasks. In the meta-training phase, first use the training set to obtain the loss value $\mathcal{L}_{\mathcal{T}_i}(f_\theta)$ of the original model parameter θ on $\mathcal{T}_i$, and then use gradient descent to obtain θ_i.

$$\theta_i = \theta - \alpha \nabla_\theta \mathcal{L}_{\mathcal{T}_i}(f_\theta) \qquad (1)$$

Where α is the meta-training learning rate used in the inner loop. Then test set D_{test} is then used to verify on the expected parameter θ_i, thus obtaining a new loss, meta loss $\mathcal{L}_{\mathcal{T}_i}(f_{\theta_i})$. The loss value here can only be regarded as a part of meta loss, and the cumulative sum of $\mathcal{L}_{\mathcal{T}_i}(f_{\theta_i})$ is calculated after the entire internal loop is the final meta loss. Calculate the gradient of the total loss and do stochastic gradient descent to update the original parameter values of the model as:

$$\theta = \theta - \beta \nabla_\theta \sum_{\mathcal{T}_i \sim p(\mathcal{T})} \mathcal{L}_{\mathcal{T}_i}(f_{\theta_i}) \qquad (2)$$

Where β is the learning rate used in the outer loop.

4. Our approach-improved MAML

The MAML network architecture was originally derived from the embedded function network architecture used by Vinyals et al [22]. This network architecture has the standard configuration of convolutional neural network commonly used in image classification tasks, as shown in Figure 1.

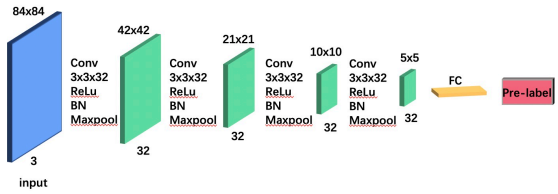

Figure 1. MAML network model

With the network model above, MAML can be directly applied for iris recognition, as demonstrated in the Experiment section. However, to generalize the model, improve the performance of the model in multi-task training and further alleviate overfitting, we improve MAML in the following two aspects:

1. As shown in Figure 1, the network model of MAML used for image classification contains four layers of convolutional neural networks. Through experiments, we have found that the following structure with addition of two more convolution modules provides the best performance on iris recognition. The composition of the two newly added modules is same as the composition of the previous modules, except that the maximum pooling process is not performed.

Figure 2. Network structure of the improved MAML

2. To reduce the over-fitting problem in the training process and improve the generalization of MAML to adapt to new tasks, we have introduced regularization constraints in the loss function, and added L2 regularization on the basis of the original cross-entropy loss, as shown in (3), where ω is the parameter for regularization.

$$L_{T_i}(f_\theta) = \sum_{x^{(j)},y^{(j)}\sim T_i} y^{(j)} log f_\theta(x^{(j)}) + (1+y^{(j)}) log(1 - f_\theta(x^{(j)})) + \frac{\lambda}{2n} \quad (3)$$

The model is represented by a parametrized function f_θ with parameters θ. When adapting to a new task $\mathcal{T}_i$, θ will become θ_i' accordingly, by taking into account the added L2 regularization constraint. A single gradient update calculation is as follows, where α is the learning rate:

$$\theta_i' = \theta - \alpha \nabla_\theta \left(\mathcal{L}_{\mathcal{T}_i}(f_\theta) + \lambda \sum_{j=1}^{n} \theta_j^2 \right) \quad (4)$$

The model parameters are trained by optimizing for the performance of $f_{\theta'}$ with respect to θ across tasks sampled from $p(\mathcal{T})$, so the meta-objective can be expressed as:

$$\min_\theta \nabla_\theta \sum_{\mathcal{T}_i\sim p(\mathcal{T})} \left(\mathcal{L}_{\mathcal{T}_i}\left(f_{\theta_i'}\right) + \lambda \sum_{j=1}^{n} \theta'^2_j \right) \quad (5)$$

The meta-optimization is performed over the model parameters θ, whereas the objective is computed using the updated model parameters θ'. By using stochastic gradient descent, the meta-optimization is performed through tasks $\mathcal{T}_i\sim p(\mathcal{T})$. Therefore, the model parameters θ are adjusted as follows:

$$\theta = \theta - \beta \nabla_\theta \sum_{\mathcal{T}_i\sim p(\mathcal{T})} \left(\mathcal{L}_{\mathcal{T}_i} + \lambda \sum_{j=1}^{n} \theta'^2_j \right) \quad (6)$$

where β represents the meta learning rate. Combing (6) with (4) gives us

$$\theta = \theta - \beta \nabla_\theta \sum_{\mathcal{T}_i\sim p(\mathcal{T})} \left(\mathcal{L}_{\mathcal{T}_i}\left(f_\theta - \alpha \nabla_\theta \mathcal{L}_{\mathcal{T}_i}(f_\theta) + \lambda \sum_{j=1}^{n} \theta_j^2 \right) + \lambda \sum_{j=1}^{n} \theta'^2_j \right) \quad (7)$$

The corresponding algorithm is outlined in Algorithm 1:

Algorithm 1 Our improved MAML

Require: Distribution of tasks $p(\mathcal{T})$, the learning rate α and β
1.Initialize θ randomly
2.**While** not done **do**
3. Sample tasks $\mathcal{T}_i$ according to $p(\mathcal{T})$
4. **for all** tasks $\mathcal{T}_i$ **do**
5. Draw K samples from $\mathcal{T}_i$: $\mathcal{D}^{val} = \{x^{(j)}, y^{(j)}\}$
6. Calculate $\nabla_\theta(\mathcal{L}_{\mathcal{T}_i}(f_\theta) + \lambda \sum \theta^2)$ with respect to K examples
7. Compute adapted parameters with gradient descent: $\theta_i' = \theta - \alpha \nabla_\theta(\mathcal{L}_{\mathcal{T}_i}(f_\theta) + \lambda \sum \theta^2)$
8. Sample datapoints from $\mathcal{T}_i$ and get $\mathcal{D}_i^{tr} = \{x^{(j)}, y^{(j)}\}$ for the meta-update
9. **end for**
10. $\theta = \theta - \beta \nabla_\theta \sum_{\mathcal{T}_i\sim p(\mathcal{T})} (\mathcal{L}_{\mathcal{T}_i}(f_\theta - \alpha \nabla_\theta \mathcal{L}_{\mathcal{T}_i}(f_\theta) + \lambda \sum \theta^2) + \lambda \sum \theta'^2_j)$
11.**end while**

5.Experiments and results

In this section, we firstly introduce the datasets used in the experiments and the parameters settings, and then conduct training and testing on the MAML, iMAML and deep learning methods for comparison.

5.1 Datasets and Parameter Settings

The iris datasets used in our experiment come from the free and open database CASIA-V4.0 of the Institute of Automation of the Chinese Academy of Sciences and the public iris image database JLU-V1.0 of Jilin University. For the CASIA-V4.0 dataset, two subsets of CASIA-Iris-Interval and CASIA-Iris-Lamp are used, with 200 sets selected respectively as the two datasets used in the experiments. Among them, the number of iris samples in each group of the

dataset made by Interval is 5, with a total of 1000 samples; the number of iris samples in each group of the dataset made by lamp is 20, with a total of 4000 samples. For JLU-V1.0, 193 groups were selected for the experiment, and each group contained 20 iris samples, totaling 3860 samples. The iris samples contained in each group of the above dataset belong to the same person, that is, each group of samples belongs to the same category.

The iris images need to be preprocessed. Firstly, the images are positioned, and then the iris images with a rectangular shape are obtained after normalization. We use the Osiris v4.1 [23] system to locate and segment the iris region. In order to retrieve the iris contour, the Viterbi algorithm [24] is applied to the gradient map of the image processed by anisotropic smoothing. The Viterbi algorithm has two resolutions: one is high resolution, which can find accurate contours; and the other is low resolution, which retrieves rough contours that can further improve the accuracy of the normalized circle. Here Osiris v4.1 uses the second one. After the segmentation is completed, as shown in Figure 3(c), the pupil and iris circle are drawn in green, and the non-iris pixels indicated by the mask are colored in red. The image in Figure 3(b) is only useful for viewing the results and not for further processing.

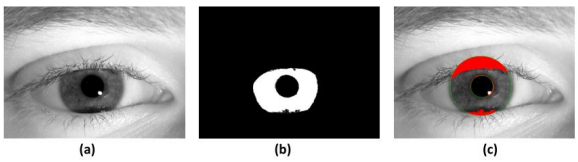

(a) original image (b) binary mask image (c) segmented image

Figure 3. Iris preprocessing for segmentation

After detecting the iris boundary, positioning and segmenting it, the iris is normalized by the Daugman's rubber-sheet model [25]. The iris normalization process mainly eliminates the problem of size inconsistency caused by the stretching of the iris area due to pupil dilation under different lighting conditions. Figure 4 shows the normalized image of the iris image.

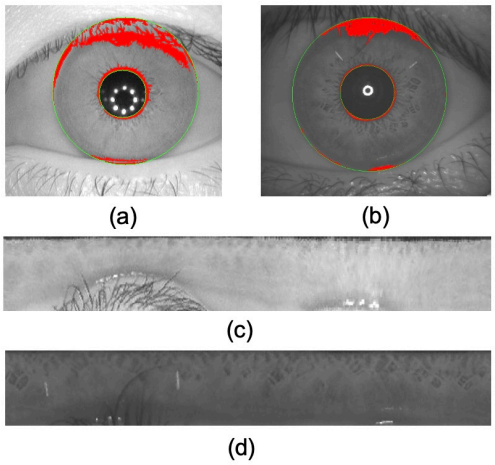

Figure 4: (a) CASIA iris image before normalization, (b) JLU iris image before normalization, (c) CASIA iris image after normalization, (d) JLU iris image after normalization.

After the iris image is normalized, the iris texture area changes from a ring to a rectangular area. Due to the preprocessing of the iris, the iris image will be affected by unfavorable factors such as acquisition light and positioning errors. Therefore, the sharpness of the normalized image is not very high, and the normalized image needs to be enhanced to increase the contrast of the image. We apply histogram equalization processing to enhance the contrast of iris image. The processed iris image sample is shown in Figure 5.

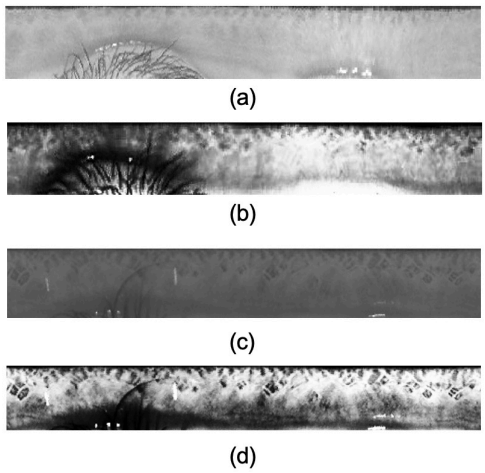

Figure 5:(a) CASIA iris image before histogram equalization, (b) CASIA Iris image after histogram equalization, (c) JLU iris image before histogram equalization, (d) JLU Iris image after histogram equalization.

5.2 Evaluation Metric

To measure and evaluate the performance of iMAML and the methods used for comparison, we use the most common neural network evaluation indicator, i.e., the accuracy rate. The accuracy rate represents the ratio of the correct number of predicted samples to the total number of samples.

5.3 Comparison of MAML and iMAML

During the experiment, the samples in each dataset are divided into three parts: training group, verification group and test group. The CASIA-Iris-Interval and CASIA-Iris-Lamp datasets have 128 groups for training, 32 groups for verification and 40 groups for testing. The number of groups used for training in the JLU-V1.0 dataset is 127, the number of groups used for verification is 30, and the number of groups used for testing is 36. Each dataset has a corresponding category label, which is stored in a csv file. The CASIA-Iris-Interval dataset is only used for 5-way 1-shot experiments due to the small size of the data, and the remaining datasets are used for 5-way 1-shot and 5-way 5-shot experiments. The 5-way 1-shot means that each task in the meta-training stage randomly selects 5 categories of iris samples, and each category selects 1 labeled sample. The 5-way 5-shot means that each task in the meta-training phase randomly selects 5 categories of iris samples, and each category selects 5 labeled samples. The preprocessed iris image is uniformly processed into a square picture with a size of 84×84. Choosing this resolution is the result of trying various sizes, details of the experiment are in section 5.5.2.

Both MAML and iMAML use the above three datasets for training. In the training phase, the number of iterations is uniformly set to 20,000 steps, and the verification is performed every 500 steps, and the meta_batch_size is uniformly set to 2, that is, one iteration contains two tasks. The specific parameter settings of the MAML and enhanced MAML training phase experiments are shown in the corresponding table 1- 4:

Table 1 MAML 5-way 1-shot experiment parameter settings

Parameter	Value
update learning rate	$1.0x10^{-2}$
number of updates	5
number of classes	5
update batch size	1
meta-batch size	2
meta learning rate	$1.0x10^{-3}$
optimizer	Adam

Table 2 MAML 5-way 5-shot experiment parameter settings

Parameter	Value
update learning rate	$1.0x10^{-2}$
number of updates	5
number of classes	5
update batch size	5
meta-batch size	2
meta learning rate	$1.0x10^{-3}$
optimizer	Adam

Table 3 iMAML 5-way 1-shot experiment parameter settings

Parameter	Value
update learning rate	0.01
number of updates	5
number of classes	5
update batch size	1
meta-batch size	2
meta learning rate	$1.0x10^{-3}$
optimizer	Adam
l2 weight	0.089

Table 4 iMAML 5-way 5-shot experiment parameter settings

Parameter	Value
update learning rate	0.09
number of updates	5
Number of classes	5
update batch size	5
meta-batch size	2
meta learning rate	$1.0x10^{-3}$
optimizer	Adam
l2 weight	0.089

Table 5 shows the results of 5-way 1-shot and 5-way 5-shot on the CASIA-Iris-Interval, CASIA-Iris-Lamp and JLU-V1.0 dataset for MAML and iMAML. It can be seen that, overall, the experimental results of the iMAML on the three datasets are better, compared with MAML. Particularly, for the 5-way 1-shot experiment of CASIA-Iris-Interval, the accuracy of iMAML is 5.39% higher than that of MAML. On the CASIA-Iris-Lamp dataset, in the 5-way 1-shot experiment, iMAML has an accuracy increase of 3.39%, compared with MAML. Since in the 5-way 5-shot experiment, each task selects 5 samples for training, the number of training samples for each type is considerably higher than the number of samples 1 for each type of 5-way 1-shot training. Therefore, overall, for both iMAML and MAML, the recognition accuracy of 5-way 5-shot in each group of experiments is higher than that of 5-way 1-shot.

Table 5 The recognition rate of MAML and iMAML on each dataset

Few-shot learning method	DataSet	Feature extractor	1-shot	5-shot
MAML	CASIA-Iris-Interval	4 Conv	93.7%	-
iMAML	CASIA-Iris-Interval	6 Conv	99.09%	-
MAML	CASIA-Iris-Lamp	4 Conv	94.4%	98.2%
iMAML	CASIA-Iris-Lamp	6 Conv	97.79%	98.9%
MAML	JLU-V1.0	4 Conv	99.59%	99.84%
iMAML	JLU-V1.0	6 Conv	99.73%	99.295%

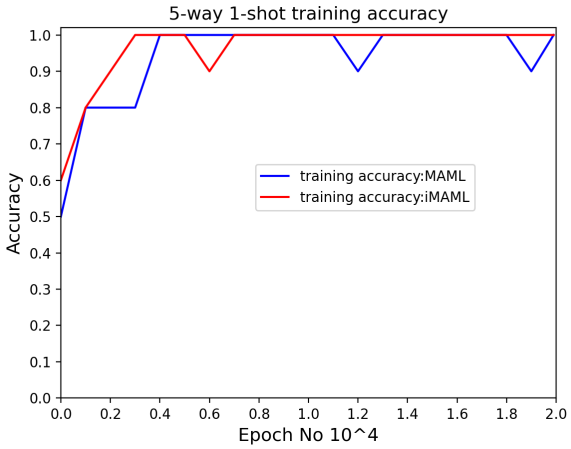

(a) on CASIA-Iris-Interval dataset

(d) on CASIA-Iris-Lamp dataset

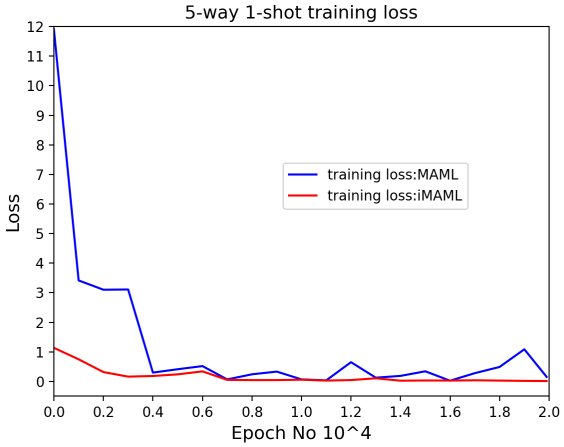

(b) on CASIA-Iris-Interval dataset

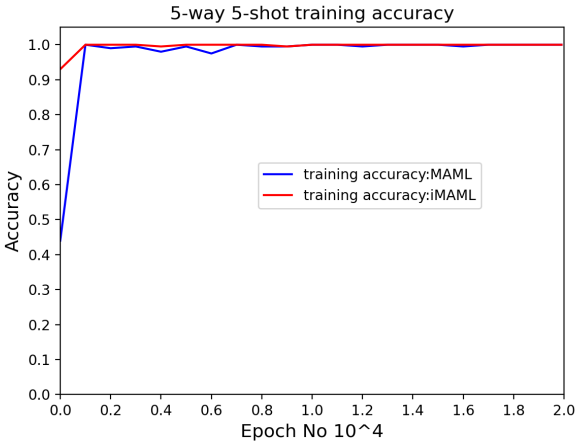

(e) on CASIA-Iris-Lamp dataset

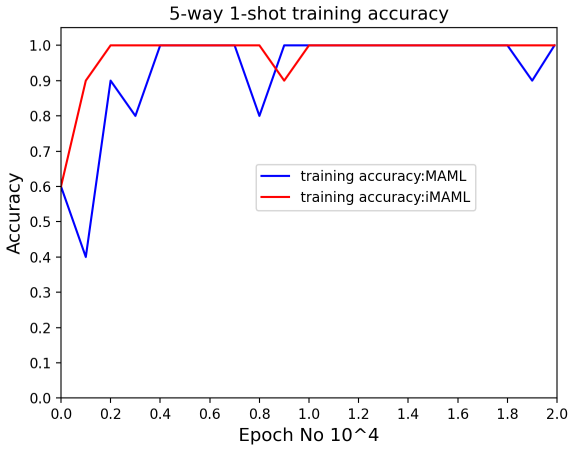

(c) on CASIA-Iris-Lamp dataset

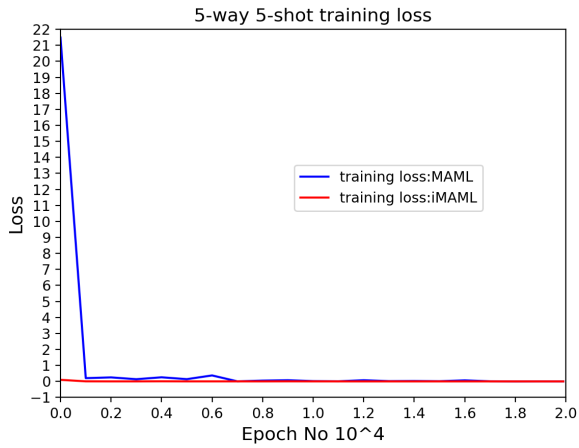

(f) on CASIA-Iris-Lamp dataset

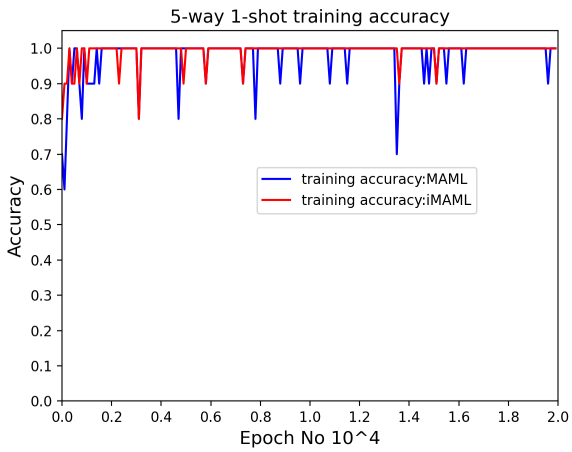

(g) on JLU-V1.0 dataset

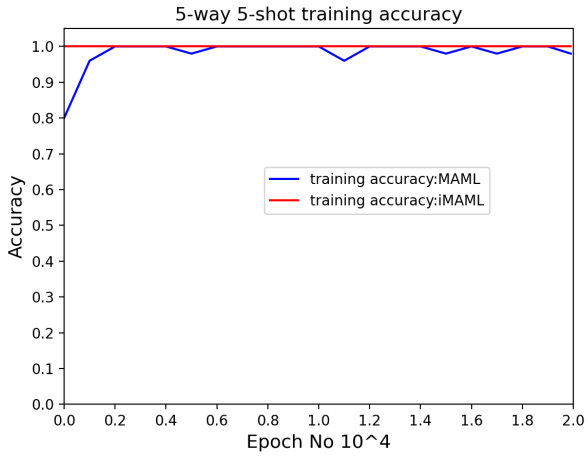

(i) on JLU-V1.0 dataset

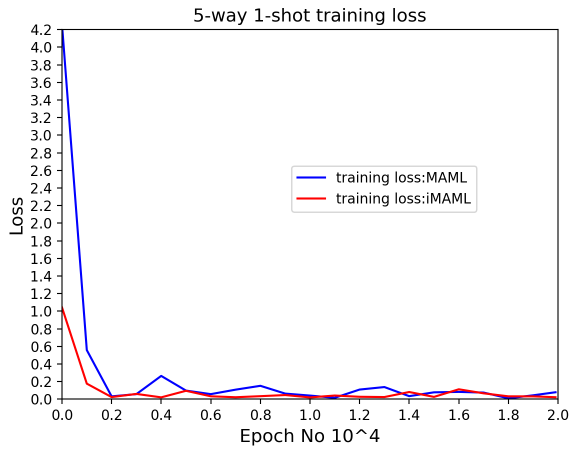

(h) on JLU-V1.0 dataset

(j) on JLU-V1.0 dataset

Figure 7. Training accuracy and loss of MAMl and iMAML for different datasets

As shown in Figure 7 above, we can see that iMAML has a more stable training accuracy and a greater fluctuation range than MAML, and it reaches the highest point more quickly. And iMAML has lower training loss than MAML as a whole, and it converges faster. This proves the effectiveness of our iMAML method.

5.4 Comparison of iMAML and Deep Learning Based Methods for Iris Recognition

In this section, we compare iMAML and a few representative deep network models that are trained and tested on small sample iris datasets. First, we preprocess the iris images using the same approach as in the section 5.2. During the training, the models extract features of iris images and use the Softmax layer to classify iris. We use the same datasets as that in section 5.2. Each group in the dataset is divided into training set, validation set and test set. Each group of CASIA-Iris-Interval dataset selects 3 training samples, one verification sample and one test sample. The number of training samples for each group of CASIA-Iris-Lamp and JLU-V1.0 dataset is 12 and we set both the verification sample and the test sample as 4. With these datasets, we use TensorFlow to train, verify and test the models for iris recognition.

The training process uses cross entropy as the loss function, and uses the stochastic gradient descent to update network parameters. The main parameters of the training phase are shown in Table 6. The image sizes used for VGG16, Inception-V3, ResNet-50, Efficientnet-b0, Mobilenet-Small, Mobilenet-Large, DeepirisNet-A and DeepirisNet-B, are uniformly processed as 224×224,299×299, 224×224, 224×224, 224×224, 128×128 and 128x128, respectively. The accuracy of recognition is given in Table 7.

Table 6 Deep learning network parameter settings

Parameter	Value
batch-size	4
learning-rate	0.01
step	20000
learning rate-reduce-patience	10

As can be seen in Table 5 and 7, the accuracy of iMAML is 99.09%, and the accuracy of MAML is 93.07%, both of which are higher than the 84.5% of the highest recognition accuracy achieved by DeepirisNet-B. For CASIA-Iris-Lamp, the accuracy of iMAML is 98.9%, and the accuracy rate of MAML is 98.2%, both are higher than the 96.87% of the highest recognition accuracy achieved by Inception-V3. And for JLU-V1.0, the accuracy achieved by iMAML is 99.95%, and the accuracy achieved by MAML is 9.84%. Both are higher than the highest accuracy rate of 98.12% achieved by DenseNet. Obviously, iMAML proposed in this paper and MAML have considerable advantages in iris recognition when small samples are available for training

Table 7 The recognition accuracy of each deep learning model

Deep Learning model	DataSet	Accuracy
VGG16	CASIA-Iris-Interval	68%
VGG16	CASIA-Iris-lamp	86%
VGG16	JLU-V1.0	87.5%
Inception-V3	CASIA-Iris-Interval	75.5%
Inception-V3	CASIA-Iris-lamp	96.87%
Inception-V3	JLU-V1.0	96.87%
ResNet-50	CASIA-Iris-Interval	80%
ResNet-50	CASIA-Iris-lamp	94.87%
ResNet-50	JLU-V1.0	95.5%
DenseNet	CASIA-Iris-Interval	80.5%

DenseNet	CASIA-Iris-lamp	96.37%
DenseNet	JLU-V1.0	98.12%
EfficientNetB0	CASIA-Iris-Interval	78.5%
EfficientNetB0	CASIA-Iris-lamp	93.75%
EfficientNetB0	JLU-V1.0	96.87%
MobileNetV3-Small	CASIA-Iris-Interval	71%
MobileNetV3-Small	CASIA-Iris-lamp	93.75%
MobileNetV3-Small	JLU-V1.0	98%
MobileNetv3-Large	CASIA-Iris-Interval	66.5%
MobileNetv3-Large	CASIA-Iris-lamp	94.5%
MobileNetv3-Large	JLU-V1.0	97.75%
DeepIrisNet-A	CASIA-Iris-Interval	73%
DeepIrisNet-A	CASIA-Iris-lamp	95.87%
DeepIrisNet-A	JLU-V1.0	97.75%
DeepIrisNet-B	CASIA-Iris-Interval	84.5%
DeepIrisNet-B	CASIA-Iris-lamp	96.75%
DeepIrisNet-B	JLU-V1.0	97.5%

5.5 Analysis of Parameters

5.5.1 Network Structure

We replaced the original MAML's network with a simple convolutional network ResNet network and Inception network, conducted experiments on the CASIA-Iris-Lamp dataset, and compared their performance with iMAML. Our experimental results below show that iMAML (with two convolutional layers) achieved the best result, as displayed in Table 8. The reason is that the MAML training strategy will lead to complex calculations. Only shallow, uncomplicated neural networks can be used as base-learners. Complex networks like ResNet and Inception are easy to overfit during training.

5.5.2 Iris Image Size

We evaluated the influence of various input Iris image sizes on the recognition accuracy, by carrying experiments on the CASIA-Iris-Interval dataset. It can be seen from the results that the size 84x84 gives the best result, and the accuracy decreases with the increase of the size. This could be due to the discriminative iris features under this size are better obtained.

Table 8 The recognition accuracy of various network structures

Few-shot learning method	DataSet	1-shot Accuracy	5-shot Accuracy
MAML(Conv6)	CASIA-Iris-Lamp	97.79%	98.9%
MAML(Conv9)	CASIA-Iris-Lamp	86.96%	97.4%
MAML(Conv12)	CASIA-Iris-Lamp	82.19%	95.98%
MAML(ResNet6)	CASIA-Iris-Lamp	84.99%	88.89%
MAML(ResNet9)	CASIA-Iris-Lamp	88.89%	96.87%
MAML(ResNet12)	CASIA-Iris-Lamp	91.3%	97.2%
MAML(Inceotion6)	CASIA-Iris-Lamp	91.03%	97.6%
MAML(Inceotion9)	CASIA-Iris-Lamp	86%	96.28%
MAML(Inceotion12)	CASIA-Iris-Lamp	88.89%	96.8%

Table 9 the Influence of Input Size on Recognition Rate (Accuracy(%))

Input size	60×60	84×84	100×100	128×128	140×140
iMAML 1-shot	96.63%	99.26%	99.06%	95.46%	94.96%

Table 10 Image Rotation Analysis

Rotation Angle (degree)	-8	-6	-4	-2	0	+2	+4	+6	+8
DeepIrisNet-A	67%	69%	72.5%	71.5%	73.5%	73.5%	71.5%	69.5%	68%
iMAML 1-shot	98.69%	98.49%	98.89%	98.99%	99.26%	98.97%	98.83%	98.89%	98.10%

5.6 Invariance to Rotation

When a person's iris was captured, the head of the person may not be aligning with the collecting device, which may cause iris rotation problems. DeepIrisNet shows excellent invariance to this change, but in the case of sufficient samples provided for tranining. To study the influence of the iris image's rotation to our method's recognition accuracy, we used the CASIA-Iris-Interval dataset and trained it with non-rotating images. During the testing process, the test images were rotated in the range of -8 degree to +8 degree with a step size of 2 degree. DeepirisNet-A is selected to perform the same steps, but with small sample size. As seen in Table 10, our iMAML achieved much better results against the rotation of iris images.

6 Conclusion

In this paper, we study the iris recognition problem with limited training data. Based on MAML algorithm in meta-learning, we introduce L2 regularization on the basis of the original cross entropy loss function of MAML to improve the generation of the approach and avoid the overfitting. At the same time, in order to further improve the ability of embedded network to extract features, we have improved the original network structure of MAML with the addition of two convolution modules.

Experimental results show that the proposed method can effectively improve the accuracy of recognition and has considerable advantages compared with deep learning methods. In the future work, we will further explore the application of other small sample learning methods in the field of iris recognition.

Acknowledgements

This work was supported by National Joint Engineering Laboratory of New Network and Detection Foundation (grant no. GSYSJ2016008), Shaanxi Science and Technology Plan Project (grant no. 2020GY-066). Portions of the research in this paper use the CASIA-Iris collected by the Chinese Academy of Sciences' Institute of Automation (CASIA) and JLU-V1.0 of Research Institute of Biometrics and Information Security Technology, Jilin University. Reference: "JLU Iris Image Database, http://biis.jlu.edu.cn/irisdatabase/".

References

1 Hajari K (2015) Improving iris recognition performance using local binary pattern and combined RBFNN. Int J Eng Adv Tech-nol 4(4):108–112

2 Tan T, Sun Z (2009) Ordinal measures for iris recognition. IEEE Trans Pattern Anal Mach Intell 31(12):2211–2226

3 Zhu, Yong, Tieniu Tan, and Yunhong Wang. "Biometric personal identification based on iris patterns." Proceedings 15th International Conference on Pattern Recognition. ICPR-2000. Vol. 2. IEEE, 2000.

4 Ibrahim, Muhammad Talal, et al. "Iris localization using local histogram and other image statistics." Optics and Lasers in Engineering 50.5 (2012): 645-654.

5 Davson, Hugh. Physiology of the Eye. Macmillan International Higher Education, 1990.

6 Gangwar A, Joshi A. DeepIrisNet: Deep iris representation with applications in iris recognition and cross-sensor iris recognition[C]//2016 IEEE international conference on image processing (ICIP). IEEE, 2016: 2301-2305.

7 Zhao T, Liu Y, Huo G, et al. A deep learning iris recognition method based on capsule network architecture[J]. IEEE Access, 2019, 7: 49691-49701.

8 Wang K, Kumar A. Cross-spectral iris recognition using CNN and supervised discrete hashing[J]. Pattern Recognition, 2019, 86: 85-98.

9 Liu N, Li H, Zhang M, et al. Accurate iris segmentation in non-cooperative environments using fully convolutional networks[C]//2016 International Conference on Biometrics (ICB). IEEE, 2016: 1-8.

10 Lu J, Gong P, Ye J, et al. Learning from Very Few Samples: A Survey[J]. arXiv preprint arXiv:2009.02653, 2020.

11 Al-Waisy A S, Qahwaji R, Ipson S, et al. A multi-biometric iris recognition system based on a deep learning approach[J]. Pattern Analysis & Applications, 2017(4): 1-20.

12 Finn C, Abbeel P, Levine S. Model-agnostic meta-learning for fast adaptation of deep networks[C]//International Conference on Machine Learning. PMLR, 2017: 1126-1135.

13 Daugman J G. High confidence visual recognition of persons by a test of statistical independence[J]. IEEE transactions on pattern analysis and machine intelligence, 1993, 15(11): 1148-1161.

14 W. W. Boles, B. Boashash. A human identification technique using images of the iris and wavelet transform[J]. IEEE Transactions on Signal Processing. 1998, 46(4):1185-1188.

15 Lim S, Lee K, Byeon O, et al. Efficient iris recognition through improvement of feature Vector and classifier [J]. ETRI Journal,23,2(2001.06.10), 2001, 23(23):61-70.

16 Li Ma, Yunhong Wang and Tieniu Tan, "Iris recognition using circular symmetric filters," Object recognition supported by user interaction for service robots, Quebec City, Quebec, Canada, 2002, pp. 414-417 vol.2

17 M. Vatsa, R. Singh, A. Ross and A. Noore, "Quality-Based Fusion for Multichannel Iris Recognition," 2010 20th International Conference on Pattern Recognition, Istanbul, 2010, pp. 1314-1317.

18 S. Minaee, A. Abdolrashidiy and Y. Wang, "An experimental study of deep convolutional features for iris recognition," 2016 IEEE Signal Processing in Medicine and Biology Symposium (SPMB), Philadelphia, PA, 2016, pp. 1-6.

19 W. Zhang, C. Wang and P. Xue, "Application of convolution neural network in Iris recognition technology," 2017 4th International Conference on Systems and Informatics (ICSAI), Hangzhou, 2017, pp. 1169-1174

20 Hinton, Geoffrey E., et al. "Improving neural networks by preventing co-adaptation of feature detectors." arXiv preprinarXiv:1207.0580 (2012).

21 Y. Wang, M. Li and H. Zhang, Ethnic classification based on iris texture depth feature and Fisher vector[J].Chinese Journal of Image and Graphics, 2018, 23(01): 28-38.

22 Vinyals O, Blundell C, Lillicrap T, Koray K. Matching networks for one shot learning. In: Proceedings of the 30th International Conference on Neural Information Processing Systems. Barcelona, Spain:MIT Press, 2016. 3630−3638

23 Sutra G, Dorizzi B, Garcia-Salicetti S, et al. A biometric reference system for iris. OSIRIS version 4.1[J]. Telecom Sud Paris, France, Tech. Rep, 2012.

24 G. Sutra, S. Garcia-Salicetti, and B. Dorizzi, "The Viterbi algorithm at different resolution for enhanced iris segmentation". 5th IAPR International Conference on Biometrics, p. 310-316, 2012.

25 Daugman, John. "How iris recognition works." The essential guide to image processing. Academic Press, 2009. 715-739.